Atmos. Chem. Phys. Discuss., 9, 19205–19241, 2009
www.atmos-chem-phys-discuss.net/9/19205/2009/

Atmospheric Chemistry and Physics Discussions

This discussion paper is/has been under review for the journal *Atmospheric Chemistry and Physics (ACP)*. Please refer to the corresponding final paper in *ACP* if available.

Constraint of anthropogenic NO_x emissions in China from different sectors: a new methodology using multiple satellite retrievals

J.-T. Lin[1], M. B. McElroy[1], and K. F. Boersma[2]

[1]School of Engineering and Applied Sciences, Harvard University, Cambridge, MA 02138, USA
[2]KNMI, Climate Observations Department, De Bilt, The Netherlands

Received: 17 July 2009 – Accepted: 17 August 2009 – Published: 16 September 2009

Correspondence to: J.-T. Lin (jlin5@seas.harvard.edu)

Published by Copernicus Publications on behalf of the European Geosciences Union.

Abstract

A new methodology is developed to constrain Chinese anthropogenic emissions of nitrogen oxides (NO_x) from four major sectors (industry, power plants, mobile and residential) in July 2008. It combines tropospheric NO_2 column retrievals from GOME-2 and OMI, taking advantage of their different passing time over China (9:30 a.m. local time versus 1:30 p.m.), and explicitly accounts for diurnal variations in anthropogenic emissions of NO_x as well as their tropospheric lifetime and column concentrations. The approach is based on the daytime variation of NO_x (when its lifetime is relatively short) alone; and potential errors in inverse modeling by neglecting horizontal transport are minimized. Separation of anthropogenic sectors relies on the estimated diurnal profiles and budget uncertainties. Our best top-down estimate suggests a national budget of 6.8 Tg N/yr (5.5 Tg N/yr for East China), close to the a priori bottom-up emission estimate from the INTEX-B mission. The top-down emissions are lower than the a priori near Beijing, in the northeastern provinces and along the east coast; yet they exceed the a priori over many inland regions. Systematic errors in satellite retrievals are estimated to lead to underestimation of top-down emissions by at most 17% (most likely 10%). Effects of other factors on the top-down estimate are typically less than 15%, including lightning, soil emissions, mixing in planetary boundary layer, anthropogenic emissions of carbon monoxide and volatile organic compounds, assumptions on emission diurnal variations, and uncertainties in the four sectors. The a posteriori emission budget is 5.7 Tg N/yr for East China.

1 Introduction

Anthropogenic emissions of nitrogen oxides ($NO_x \equiv NO+NO_2$) in China have been under intensive study (Streets et al., 2003; Wang et al., 2004, 2007; Zhang et al., 2007, 2009; van der A et al., 2008; Zhao and Wang, 2009) in response to their fast growth and significant contributions to air pollution in source and downwind regions (Wuebbles

ACPD

9, 19205–19241, 2009

et al., 2007; Lin et al., 2008a; Zhang et al., 2008). The bottom-up emission estimation requires information on emission-related activities and emission factors, subject often to large uncertainties in relevant statistics and measurements (Zhang et al., 2007). Inverse modeling incorporating chemical transport models (CTMs) and measurements of nitrogen species offers valuable information for constraining NO_x emissions (Wang et al., 2004).

Remote sensing instruments onboard several satellites provide snapshots of tropospheric NO_2 at different times of day over China, with much better spatial coverage than ground-based or in situ measurements. Thus, top-down constraints incorporating satellite remote sensing and CTMs have attracted particular attention. Martin et al. (2003) introduced a simple method (referred to as "Martin et al. method" hereafter) proportioning retrieved tropospheric NO_2 columns to local NO_x emissions. With this method, horizontal transport is neglected given the short tropospheric lifetime of NO_x over polluted areas (3–10 h, shorter in summer) such that the impacts of horizontal transport can be neglected at the scale of a GEOS-Chem gridcell of $2^\circ \times 2.5^\circ$. Diurnal variations of NO_x emissions and lifetime are accounted for implicitly in the CTM. Impacts of nighttime evolution of NO_x (when its lifetime is much longer so that neglecting horizontal transport may introduce errors in the inverse modeling) are not excluded (see more analysis in Sect. 2.4). This method was applied widely later to satellite retrievals from GOME or SCIAMACHY for deriving monthly emissions (Jaeglé et al., 2005; Martin et al., 2006; Wang et al., 2007). Zhang et al. (2007) found that such top-down estimations often suggest much higher Chinese emissions than results from the bottom-up approach. Zhao and Wang (2009) applied the same method to a regional model (grid size is ~70 km) over East Asia for daily assimilation of anthropogenic emissions, as constrained by the OMI NO_2 retrieval. In their study, impacts of horizontal transport on their relatively fine resolution were assumed to be accounted for indirectly by daily assimilation (Y. Wang, personal communication). All these top-down studies do not partition top-down anthropogenic emissions to individual sectors.

In this study, a new inverse modeling method is proposed to constrain Chinese an-

ACPD
9, 19205–19241, 2009

thropogenic emissions of NO_x from four major sectors (industry, power plants, mobile and residential). It combines NO_2 retrievals from OMI and the newly available GOME-2, using the global GEOS-Chem CTM to link emissions to tropospheric columns. OMI and GOME-2 retrievals provide significantly improved spatial and temporal coverage as compared to GOME and SCIAMACHY. Anthropogenic emissions for the year of 2006 from the INTEX-B mission (Zhang et al., 2009) are used as a priori. Results are presented here for July 2008 in place of 2006, since the meteorology for 2006 was not available at the time this study was conducted, and the GOME-2 retrieval is available only after March 2007.

Section 2 provides brief descriptions of satellite NO_2 retrievals and GEOS-Chem simulations and introduces the new top-down approach. Comparisons of retrieved and simulated tropospheric NO_2 columns are presented in Sect. 3. Sections 4 and 5 present our best top-down estimate of Chinese anthropogenic emissions, together with a suite of uncertainty analyses, and the corresponding a posteriori emissions. Section 6 concludes the present study.

2 Methodology

2.1 GOME-2 and OMI retrievals

Level-2 retrievals of GOME-2 and OMI are derived by KNMI (Boersma et al., 2004; Boersma et al., 2007). Readers are referred to the Product Specification Document (Boersma et al., 2009a) for more information on the datasets. The OMI retrieval has been successfully validated (Boersma et al., 2008a, b), and GOME-2 compares well with SCIAMACHY (Mijling et al., 2009) that has been validated by Blond et al. (2007) and Boersma et al. (2009b). Figure 1a also indicates a good consistency in monthly mean retrievals between GOME-2 and SCIAMACHY over East China (103.75°–123.75° E, 19°–45° N) in July 2008, with a slope of 0.90 and a R^2 of 0.91 using the Reduced Major Axis (RMA) regression. Table 1 presents key retrieval pa-

ACPD
9, 19205–19241, 2009

rameters for the two instruments. Daily retrievals (viewing pixels with cloud radiance fractions <50%, i.e., cloud fraction <15%) are gridded to 2° lat×2.5° lon. Monthly mean NO_2 columns (Fig. 2) are calculated by averaging results for days when GOME-2 and OMI are both available.

One difference between the GOME-2 and OMI instruments is the size of viewing pixels, which is 40 km×80 km and 13 km×24 km, respectively, at nadir view. However, since both retrievals are gridded to a resolution of about 200 km×250 km in the present study, differences between the native resolutions of the two retrievals are not expected to have significant impacts on the results presented here. If we were to compare the two retrievals at a finer resolution, the pixel size difference might become a more important issue.

Retrievals of tropospheric NO_2 vertical column densities (VCDs) from GOME-2 and OMI use essentially the same method by KNMI, although some differences exist as a result of the unique properties of the two instruments (Boersma et al., 2004, 2007). Differences in retrieval errors between the two instruments are minimized in this case, as discussed below. Three major steps are involved in deriving the VCD from the reflectance of UV/Vis solar radiation from the Earth atmosphere measured by either instrument. First, the reflectance is converted to slant column densities (SCDs) of NO_2 by fitting the absorption cross-section spectra of NO_2 and other reference spectra to the observed reflectance spectra using the Differential Optical Absorption Spectroscopy (DOAS) technique. The temperature dependence of the NO_2 absorption cross-section spectra is taken into account in both retrievals, by using temperature profiles from ECMWF. The SCD in the troposphere is derived then by subtracting the stratospheric portion from the total SCD. The stratospheric SCD is derived by model assimilation using the same global CTM TM4 for both retrievals. Finally, the tropospheric SCD is divided by the estimated tropospheric air mass factor (AMF) to derive the tropospheric VCD. The AMF is calculated by the same radiative transport model for both GOME-2 and OMI. It is determined by many factors including solar and viewing zenith angles, (effective) cloud fraction and cloud pressure, surface albedo and pressure, and the

ACPD
9, 19205–19241, 2009

a priori vertical profile of NO_2. The a priori NO_2 profile is derived from TM4, sampled at 09:30 a.m. local time for GOME-2, and at 1:30 p.m. for OMI, to account for the growth of the atmospheric boundary layer depth between 09:30 a.m. and 1:30 p.m. and the greater vertical extent of NO_2 seen by OMI. The vertical mixing difference has been shown to lead to ~15% higher AMF for OMI (Boersma et al., 2008b).

Errors in the retrieved VCD of tropospheric NO_2 are derived from errors in total SCD, its stratospheric portion, and the tropospheric AMF. These errors are discussed briefly below. Readers are referred to Boersma et al. (2004, 2007, 2008a, b) for detailed error analysis. Direct error analysis for the GOME-2 retrieval is not available at present and is out of the scope of this study. Due to its similarity to GOME and SCIAMACHY (overpass time, exactly the same retrieval method (including cloud scheme), etc.), we estimate that its error is close to GOME and SCIAMACHY. Thus the error estimation for GOME-2 presented here adopts values from previous studies for GOME and SCIAMACHY, unless indicated otherwise. Errors in the SCD are estimated at $\sim 0.5\times10^{15}$ molec/cm^2 for GOME-2 and $\sim 0.7\times10^{15}$ molec/cm^2 for OMI, which are relatively small compared to the tropospheric VCD over polluted regions like East China. Errors in the stratospheric SCD are also relatively small, at a magnitude of $\leq 0.3\times10^{15}$ molec/cm^2 for both GOME-2 and OMI. Therefore, over East China, errors in the retrieved tropospheric VCD are attributed mainly to the calculation of AMF. Retrieval errors due to inaccuracies in the a priori vertical profile of NO_2 are estimated at ~10% for both GOME-2 and OMI. These errors are removed in this study by applying the averaging kernel to the modeled vertical profile of NO_2. Errors in cloud fraction, which are estimated at 5% or less, can lead to up to 30% error in the retrieved VCD. Like GOME and SCIAMACHY retrievals, GOME-2 adopts the FRESCO+ scheme (Wang et al., 2008) for cloud retrieval, by comparing the reflectance measured inside and outside of the strong oxygen A band (758–766 nm). By comparison, the OMI retrieval utilizes the weakly absorbing O_2–O_2 band at 477 nm for cloud retrieval (Acarreta et al., 2004). Comparisons of the two cloud retrieval schemes at the same time of day are not available since there is no sensor flying at 1:30 p.m. with O2-A band

ACPD
9, 19205–19241, 2009

capability. Boersma et al. (2007) compared the two cloud schemes relative to the time of SCIAMACHY (overpass time is ~10:00 a.m. local time) and OMI, respectively. They found that, average over 5–11 August 2006, the retrieved cloud fraction differs ~1% between the two schemes. Cloud pressure is derived simultaneously with cloud fraction. Boersma et al. (2007) found that cloud pressure relative to OMI (using the O_2–O_2 band) is ~60 hPa larger than that for SCIAMACHY (using the FRESCO scheme), since the O_2–O_2 band is more sensitive to the lower troposphere. For GOME-2, errors in cloud pressure are estimated to contribute only ~2% to the VCD error, since the cloud top is typically above the lowest troposphere where NO_2 concentrates. For OMI, clouds are lower and closer to the polluted layer, and errors in cloud pressure can lead to ~15% error in the VCD retrieval. The presence of aerosols also influences the NO_2 reflectance. In the KNMI approach used here, the effects of aerosols are accounted for indirectly in the cloud retrieval scheme (Boersma et al., 2004, 2007). Errors in surface albedo are also an important source of retrieval error. Both GOME-2 and OMI retrievals make use of, in the same manner, surface albedo databases from TOMS at 380 nm and databases from GOME at both 380 nm and 440 nm. Also, both retrievals use surface pressure data at corresponding times of day from ECMWF at the resolution of TM4 ($3^\circ \times 2^\circ$).

Retrieval errors are composed of both systematic and random errors (Boersma et al., 2004, 2007). Averaged over a long time period (e.g., a month) and large area (e.g., East China), the random error is reduced to a level relatively small as compared to the systematic error (which is not affected by the averaging). Since GOME-2 and OMI retrievals are derived with a very similar methodology, systematic errors in the two retrievals are expected to correlate positively with each other. Thus the difference between the two retrievals is able to provide valuable information on the emission and chemical evolution of NO_x in between the overpass times of the two instruments. Indeed, Boersma et al. (2008b) found that, all over the world, differences between SCIAMACHY and OMI reflect largely the temporal variation of NO_x chemistry and emissions. Such temporal variation has been validated by independent measurements over the

ACPD
9, 19205–19241, 2009

Middle East (Israeli cities and the Cairo region), where both space-based measurements and ground-based observations indicated strongest diurnal cycle in summer (with strong photochemistry) and little difference between 10:00 a.m. and 1:30 p.m. in winter (Boersma et al., 2009b).

The consistency between GOME-2 and OMI retrievals is analyzed further by investigating their spatiotemporal correlation. The monthly mean NO_2 VCD has a large spatial correlation between GOME-2 and OMI, with a R^2 of 0.81 over East China (Fig. 1b). Additionally, the regional mean VCDs over East China from GOME-2 and OMI vary temporally with each other with a day-to-day correlation coefficient of 0.74 for July 2008 (Fig. 3a). The consistency is attributable partially to the similar methodology used for deriving GOME-2 and OMI retrievals.

Systematic errors in GOME-2 and OMI may differ in magnitude. Due to differences in instrument properties (viewing geometry, radiation spectra, overpass time, etc.), inaccuracies at contain steps of retrieval process may lead to different magnitudes of systematic error for the two retrievals. Moreover, the two retrievals differ in the cloud scheme, especially for cloud pressure. Impacts of such situation are analyzed further in Sect. 5.

2.2 GEOS-Chem

GEOS-Chem (v08-01-01; http://acmg.seas.harvard.edu/geos/index.html), with a horizontal resolution of 2°×2.5° and 47 layers in the vertical (~130 m for each of the 10 lowest layers), is driven by GEOS-5 from the NASA Global Modeling and Assimilation Office. The assumption of full mixing within the planetary boundary layer (PBL) in the standard model is replaced with a more realistic non-local mixing scheme formulated by Holtslag and Boville (1993) (see Lin et al., 2008b). Our preliminary analysis with GEOS-Chem indicates that the non-local scheme improves the simulation of vertical profile of NO_x in the lower troposphere, as compared with aircraft measurements from the ICARTT campaign in summer 2004. It also leads to a much better simulation of GEOS-Chem on the diurnal variation of surface ozone mixing ratio over the US, con-

ACPD
9, 19205–19241, 2009

sistent with the findings of Lin et al. (2008b).

Anthropogenic emissions over Asia for the year of 2006 from the INTEX-B mission (Zhang et al., 2009) are used as a priori. Seasonal variation is not resolved in this dataset. Also, anthropogenic emissions are assumed as constant over the course of a day when used in GEOS-Chem simulations, unless indicated otherwise. Soil NO_x emissions are specified using the scheme introduced by Yienger and Levy (1995). Lightning emissions follow Price et al. (1997), with a "C" shape profile proposed by Pickering et al. (1998). Additionally, the monthly climatology for 1995–2005 based on the OTD/LIS measurements is superimposed for the monthly flash rate budget, while the flash rate within the month is allowed to vary with convection (Sauvage et al., 2007; Lee Murray, manuscript in preparation). Biomass burning and aircraft emissions are from the GFED-2 and GEIA datasets, respectively; the relative emissions are small compared with other sources of NO_x over China in July 2008.

2.3 The new top-down approach

Our new approach is based on that satellite instruments passing China at different times of day observe and provide meaningful information on tropospheric NO_2 at different states that can be used for analyzing temporal variation of NO_x emissions and chemistry.

Neglecting horizontal transport, the temporal variation of tropospheric NO_x column for a given model gridcell is determined by

$$\partial\Omega_{NO_x}/\partial t = E - \Omega_{NO_x}/\tau \quad (1)$$

where Ω_{NO_x} is the tropospheric column of NO_x, E the total NO_x emissions, and τ the NO_x lifetime (as a result of all chemical loss processes). Assuming E and τ are constant from the i-th to i+1-th hour of the day, Eq. (1) can be used to evaluate the NO_x column at the i+1-th hour, $\Omega_{NO_x}|_{i+1}$, in terms of emissions from the i-th to i+1-th hour, E_i, and the column at the i-th hour, $\Omega_{NO_x}|_i$:

$$\Omega_{NO_x}|_{i+1} = E_i \cdot \tau_i \cdot (1 - e^{-\Delta t/\tau_i}) + \Omega_{NO_x}|_i \cdot e^{-\Delta t/\tau_i} \quad (2)$$

ACPD
9, 19205–19241, 2009

where Δt is the time interval (1 h). Integrating Eq. (2) from the 0-th to n-th hour, we find:

$$\Omega_{\mathrm{NO_x}}|_n = \overline{E} \cdot \sum_{i=0}^{n-1} (V_i \cdot \Lambda_i) + \Omega_{\mathrm{NO_x}}|_0 \cdot \mathrm{e}^{\sum_{i=1}^{n-1}(-\Delta t/\tau_i)} \quad (3)$$

where

$$V_i = E_i/\overline{E} \quad \text{and} \quad \Lambda_i = (1 - \mathrm{e}^{-\Delta t/\tau_i}) \cdot \tau_i \cdot \mathrm{e}^{\sum_{j=i+1}^{n-1}(-\Delta t/\tau_j)}$$

Here V and $\overline{E}$ define the temporal variation and daily mean of E, respectively. Equation (3) derives the dependence of the NO_x column on emissions and lifetime, subject only to assumptions in Eq. (1). In analyzing the satellite data, we assume

$$\Omega_{\mathrm{NO_x,r}}/\Omega_{\mathrm{NO_2,r}} = \Omega_{\mathrm{NO_x,a}}/\Omega_{\mathrm{NO_2,a}} \quad \text{and} \quad \tau_\mathrm{r} = \tau_\mathrm{a} = \tau \quad (4)$$

Here the subscripts "r" and "a" indicate the retrieval and the model results, respectively; and $\Omega_{\mathrm{NO_x,r}}$ represents the virtually "retrieved" NO_x column. GEOS-Chem is run once and only once to calculate $\Omega_{\mathrm{NO_x,a}}/\Omega_{\mathrm{NO_2,a}}$ and τ_a. (Note that τ_a is the result of all chemical loss processes (HNO_3 and PAN formation, etc.); it is derived at every one hour by applying Eq. (2) to GEOS-Chem modeled NO_x concentration and emissions.) These results, together with $\Omega_{\mathrm{NO_2,r}}$, are used to derive $\Omega_{\mathrm{NO_x,r}}$ and its temporal variation (Eq. 5, based on Eq. 3). Note the averaging kernel is applied to $\Omega_{\mathrm{NO_2,a}}$ to remove errors associated with the assumed NO_2 profile in the retrievals (Boersma et al., 2004). It follows that

$$\Omega_{\mathrm{NO_x,r}}|_n = \overline{E}_\mathrm{r} \cdot \sum_{i=0}^{n-1} \left(V_{r,i} \cdot \Lambda_i\right) + \Omega_{\mathrm{NO_x,r}}|_0 \cdot \mathrm{e}^{\sum_{i=1}^{n-1}(-\Delta t/\tau_i)} \quad (5)$$

$$\Rightarrow \overline{E}_\mathrm{r} = \left(\Omega_{\mathrm{NO_x,r}}|_n - \Omega_{\mathrm{NO_x,r}}|_0 \cdot \mathrm{e}^{\sum_{i=1}^{n-1}(-\Delta t/\tau_i)}\right) \Big/ \sum_{i=0}^{n-1} \left(V_{r,i} \cdot \Lambda_i\right) \quad (6)$$

ACPD
9, 19205–19241, 2009

Here E_r is the "retrieved" top-down total NO_x emissions; and $\Omega_{NO_x,r}|_n - \Omega_{NO_x,r}|_0 \cdot e^{\sum_{i=1}^{n-1}(-\Delta t/\tau_i)}$ is a weighted difference between the "retrieved" NO_x columns at different times of day. Based on Eq. (6), all four sectors of anthropogenic emissions are constrained simultaneously by iteration, which finishes in seconds. At the m^{th} iteration,

$$V_{r;m,i} = E_{r;m-1,i}/\overline{E}_{r;m-1} = \left(\sum_{s=1}^{4}\left(\overline{EA}_{r;s;m-1}\cdot VA_{s,i}\right) + EO_i\right) \Big/ \left(\sum_{s=1}^{4}\left(\overline{EA}_{r;s;m-1}\right) + \overline{EO}\right) \quad (7)$$

$$\overline{E}_{r;m} = \left(\Omega_{NO_x,r}|_n - \Omega_{NO_x,r}|_0 \cdot e^{\sum_{i=1}^{n-1}(-\Delta t/\tau_i)}\right) \Big/ \sum_{i=0}^{n-1}\left(V_{r;m,i}\cdot\Lambda_i\right) \quad (8)$$

$$\overline{EA}_{r;m} = \overline{E}_{r;m} - \overline{EO} \quad (9)$$

Here EA indicates the magnitude of anthropogenic NO_x emissions with the diurnal profile of VA (VA is independent of the assumed diurnal variation in GEOS-Chem; see below), with the subscript "s" referring to the four sectors. EO refers to other emissions together, and is independent of the iteration (see below). Similar to $\overline{E}$, variables with overhead bars represent daily means. $V_{r;m,i}$ varies with $\overline{EA}_{r;s;m-1}$ in each iteration. The difference in EA_r between the m-th and $m-1$-th iteration, $\left(\overline{EA}_{r;m} - \overline{EA}_{r;m-1}\right)$, is partitioned then to individual anthropogenic sectors, assuming that the same portion of the absolute error for each sector contributes to the difference:

$$\left(\overline{EA}_{r;s;m} - \overline{EA}_{r;s;m-1}\right) / \left(U_s \cdot \overline{EA}_{r;s;m-1}\right) = c \quad (10)$$

$$\sum_{s=1}^{4}\left(\overline{EA}_{r;s;m} - \overline{EA}_{r;s;m-1}\right) = \overline{EA}_{r;m} - \overline{EA}_{r;m-1} \quad (11)$$

Here U refers to the relative uncertainty assumed for $\overline{EA}$ (see below), and c is constant

ACPD
9, 19205–19241, 2009

at each iteration and decreases with subsequent iterations. The iteration converges when

$$\left| \frac{\overline{EA}_{r;m}}{\overline{EA}_{r;m}} - 1 \right| \leq 5\% \quad (12)$$

The relatively loose criterium results from the consideration of large errors and/or uncertainties in both retrievals and model simulations. It has little effect on the top-down estimate. The iteration is initiated using Eq. (7), with daily mean a priori anthropogenic emissions serving as the initial guess for daily mean top-down emissions:

$$\overline{EA}_{r;s;0} = \overline{EA}_{a;s} \quad (13)$$

To avoid the influence of horizontal transport in the nighttime, the two satellite retrievals are applied only to calculate top-down emissions from 10:00 a.m. (local time) to 2:00 p.m., i.e., $\Omega_{NO_x,r}|_n$ corresponds to OMI and $\Omega_{NO_x,r}|_0$ to GOME-2 (and thus n=4). The diurnal variations assumed for the relevant emission sectors aforementioned are used then to generate emissions for other times of day. The overpass time of GOME-2 and OMI for a given model gridcell is ~9:30 a.m. and ~1:30 p.m., respectively. Due to the large viewing swath of both instruments (1500 km and 2600 km, respectively), the local time of a viewing pixel can depart from the overpass time by as large as ~0.6 h for GOME-2 and ~1.1 h for OMI at 45° N. However, for most viewing pixels included in this study, the local time departs from the overpass time by ≤0.5 h. Furthermore, modeled columns at 10:00 a.m. and 2:00 p.m. are used for the top-down estimate, as the model chemistry is resolved only every 1 h. Overall, the small time difference in retrievals and model results has little impact on our findings; several tests by increasing (decreasing) the time span n from 4 h to 5 h (3 h) lead to ≤3% changes in the top-down anthropogenic emission budget.

Our goal is to constrain emissions for individual anthropogenic sectors. For our best estimate, one important step is to constrain natural emissions. Lightning emissions of

ACPD
9, 19205–19241, 2009

NO_x, including their hourly variation, are assumed to represent the real world and not adjusted. NO_x emissions from biomass burning and aircraft are held constant given their relatively small contribution. Soil NO_x emissions specified using the Yienger and Levy (1995) scheme are thought to be too low by a factor of 2–3 (Wang et al., 2004; Jaeglé et al., 2005; Wang et al., 2007; Zhao and Wang, 2009) in China, due likely to an underestimate of the sources associated with fertilization and human/animal food chain (Wang et al., 2004; McElroy and Wang, 2005). They are doubled therefore for purposes of the top-down constraint.

Estimates are as follows for diurnal profiles (*VA*) of individual anthropogenic sectors necessary for separating their contributions to the top-down emissions. As shown in Fig. 4, diurnal variations follow previous surveys in Beijing (Yu Zhao, personal communication) for power plant and mobile sources, and (Wang et al., 2005) for residential. The diurnal variation for industry is assumed the same as for power plants in the absence of better information (industry consumes ~70% of electricity in China). It is worth clarifying that *VA* is completely independent of the diurnal profiles assumed in GEOS-Chem. Although anthropogenic emissions do not change within a day in GEOS-Chem simulations, they are assumed to vary according to diurnal profiles presented above when used in our new approach for deriving top-down emissions. Impacts of assuming zero diurnal variation in GEOS-Chem simulations are analyzed in Sect. 5 (sensitivity case (12); Table 2).

Meanwhile, partitioning top-down anthropogenic emissions to different sectors requires information on the relative uncertainties in their budgets (*U*). Streets et al. (2003) and Zhang et al. (2007) suggested uncertainties in Chinese emission budgets of 50%, 37%, 50%, and 164% for the four sectors, respectively. In the absence of more detailed information, these estimates of uncertainty are tentatively increased here, by 8%, to 58%, 43%, 58%, 191%, respectively, to account for potential emission differences between 2006 and 2008; they are applied then at all locations. This increase is set to be consistent with the recent annual emission increase rate of 8% (Zhao and Wang, 2009). It does not affect the partitioning, since the uncertainties are used only

ACPD
9, 19205–19241, 2009

in a relative sense (Eq. 10).

Note that top-down emissions for the four anthropogenic sectors are not completely independent, in that they share the same sign of change upon the a priori, as determined by differences between total top-down anthropogenic emissions and a priori.

2.4 Comparison with the Martin et al. method

The Martin et al. method assumes a linear relationship between NO_2 columns and NO_x emissions. It equates the ratio of the top-down to the a priori daily mean emissions to the ratio of the retrieved to the modeled NO_2 column at a particular time of day. Only a single retrieval is used for each top-down constraint, and results using retrievals at different times of day often differ (Mijling et al., 2009; and see Sect. 4). Diurnal profiles of NO_x emissions use the pre-determined values in CTMs, regardless of that CTMs are obliged often to include relatively arbitrary assumptions on emission diurnal variations in China, e.g., the standard GEOS-Chem applies the US Environmental Protection Agency (EPA) 1989 estimation to China.

The Martin et al. method represents a special case of the present approach. It can be derived using Eqs. (4) and (6), where $\Omega_{NO_x,r}|_n$ equals $\Omega_{NO_x,r}|_0$(i.e., integrating throughout the day so that n=24) and $V_{r,i}$ adopts the pre-determined values in the model (thus iterations are not necessary). In this case, however, the integration has to include the nighttime regime, when τ is relatively large and thus neglecting the horizontal transport may not be appropriate.

3 Tropospheric NO_2 column

Figure 2 illustrates retrieved and modeled monthly mean spatial distributions of tropospheric NO_2 columns over China. Both retrievals maximize over northern East China, reflecting the influence of the intensive industrialization and urbanization in this region. Peak columns in GOME-2 exceed 2×10 molec/cm^2. Local hot spots can be seen also

ACPD
9, 19205–19241, 2009

over the southern provinces. Over most western regions, NO_2 columns are typically less than 10 molec/cm^2. Additionally, the OMI retrieval is typically lower than GOME-2 over the eastern provinces, primarily due to the short lifetime of NO_x during daytime. GEOS-Chem captures the general spatial patterns of both retrievals over the eastern provinces; the absolute values of the modeled column are typically lower than the retrievals.

The coarse horizontal resolution is not found as a major factor for the model-retrieval differences. Our test at a much higher resolution (0.5° lat×0.667° lon), using the nested version of GEOS-Chem (Chen et al., 2009), indicated negative model biases relative to retrievals with a magnitude similar to the coarse resolution investigated here.

The top-down approach assumes that differences in monthly mean NO_2 columns between the retrieval and the model reflect systematic biases in the a priori emissions, rather than errors in the meteorological fields and the model. Therefore the modeled NO_2 column, irrespective of biases in the a priori assumptions, should be correlated fairly closely to the retrieval on the daily basis. This is a key factor in ensuring that the top-down approach provides useful information for evaluating the a priori. Figure 3 examines the correlations between daily variations of retrieved and modeled NO_2 columns over several regions over East China. The correlations are relatively high, suggesting that the top-down estimation is indeed informative.

4 Top-down emissions: best estimate

Our best top-down estimate of total anthropogenic emissions is compared with the a priori assumptions in Fig. 5 and Table 2, together with the comparisons for individual sectors. Diurnal variation of the top-down emissions for East China (103.75°–123.75° E, 19°–45° N) is shown in Fig. 4. Differences between the two datasets are attributed to three factors. First, they represent two different years: 2006 versus 2008. Chinese emissions differ in these two years due to the rapid pace of industrialization (the Gross Domestic Product increases by ~10% per year), offset to some extent by

ACPD
9, 19205–19241, 2009

extensive efforts to reduce emissions (targeting the 11P^{thP} 5-year plan and the 2008 Beijing Olympics). The second factor is the uncertainties in the a priori emissions. Third, the top-down approach is subject to uncertainties relating to errors in satellite retrievals, GEOS-Chem and methodology (see Sect. 5). Random retrieval errors are particularly significant over western regions where retrieved columns are typically less than 10^{15} molec/cm^2. Top-down emissions in these regions are thus not calculated using the present methodology, but are rather set equal to the a priori values.

The general spatial pattern of the top-down emissions is similar to the a priori (Fig. 5), with highest emissions in the Shanghai area followed by northern East China with several local hot spots in other regions. The total top-down budget implies a source of 5.5 Tg N/yr over East China (Table 2), as compared to 5.7 Tg N/yr in the a priori. The national budgets are 6.8 Tg N/yr and 6.6 Tg N/yr for the top-down and the a priori, respectively. However, significant differences exist between the two datasets in the spatial distribution (Fig. 6a). The top-down emissions are often smaller than the a priori along the east coast and over the industrial regions of the three northeastern provinces. The 15–50% lower emissions near Beijing may be due partially to the measures implemented there to reduce emissions in advance of the Olympics; Mijling et al. (2009) reached a similar conclusion. The lower emissions in the northeast may be related to recent efforts to reduce pollution by shutting down heavily polluting factories and by associated restructuring of industry. On the other hand, the top-down emissions exceed the a priori over many inland regions in the east. One particular region is the southern boundary of Inner-Mongolia Province, where significant numbers of large coal-fired power plants are being installed (Zhang et al., 2009). Over central East China (103°–118° E, 25°–33° N), our assumption of doubling soil emissions appears inadequate to compensate for the likely underestimation of a factor of 3 suggested by Wang et al. (2004).

Despite the larger NO_2 columns in GOME-2 and OMI retrievals than the modeled columns, our best top-down estimate suggests an emission budget similar to the a priori assumption. One apparent cause is that soil emissions are doubled for deriving the

ACPD
9, 19205–19241, 2009

top-down anthropogenic emissions. This leads to ~10% less top-down anthropogenic emissions than if soil emissions were kept unchanged. The other, and most important, cause is that the top-down emissions are determined by the weighted difference between the "retrieved" NO_x columns corresponding to GOME-2 and OMI, and not necessarily directly by either column (Eq. 6). In other words, the top-down estimate is based on changes in the "retrieved" NO_x columns. As such, the relationship between the magnitude of NO_2 retrievals and the magnitude of top-down emissions become non-linear, unlike that with the Martin et al. method. Meanwhile, impacts of errors in individual retrievals on the top-down estimate may become less important, e.g., part of retrieval errors in GOME-2 and OMI may be canceled out by utilizing differences between the retrieved columns. Averaged over China, the weighted difference between the two "retrieved" NO_x columns does not depart much from the weighted difference between the modeled columns at corresponding times. This leads to small differences between top-down and a priori emission budgets. That higher retrievals may not lead to higher top-down emissions is a unique characteristic of our approach that is worth highlighting. The impacts of retrieval errors are analyzed further in Sect. 5.

By comparison, the Martin et al. method leads to much higher top-down anthropogenic emissions than the a priori over most eastern regions (Fig. 7). The derived emission budget from all sources for East China is 10.1 Tg N/yr using GOME-2 for constraint and 8.9 Tg N/yr using OMI. Assuming soil emissions are doubled, the corresponding budgets for anthropogenic sources are 8.5 Tg N/yr (~50% higher than the a priori) using GOME-2 for constraint, in contrast to 7.3 Tg N/yr (~29% higher) using OMI.

5 Uncertainties in the top-down emissions

Uncertainties in the present top-down estimate may be attributed to a number of factors, the influences of which were evaluated in a series of sensitivity tests (see Table 2).

The first factor relates to systematic and random errors in the retrievals, which to-

ACPD
9, 19205–19241, 2009

gether are about 30–100% over East China (Boersma et al., 2004; Boersma et al., 2007). Random errors in GOME-2 and OMI retrievals may not contribute significantly to the top-down emission budget for China. Systematic errors in both retrievals are most likely of high and positive correlation with each other, while their magnitudes may differ to some extent. This difference is expected to contribute partially to that the GOME-2 retrieval leads to 13% higher total top-down emission budget than OMI using the Martin et al. method. (Another factor contributing to the 13% difference may be errors in modeled columns at the time of GOME-2 and OMI overpass.) Here three sensitivity tests were conducted for evaluating the situation where systematic errors in GOME-2 and OMI differ (Table 2). In the first test (case 6), the 13% difference was assumed to be contributed only by differences between GOME-2 and OMI retrievals. Thus the GOME-2 retrieval was scaled down by a factor of 113% (so that the Martin et al. method produces the same top-down emission budget using either GOME-2 or OMI), and the top-down emissions were re-calculated using our approach. We chose to reduce the GOME-2 retrieval instead of enhancing the OMI retrieval because the OMI retrieval is estimated to have overestimated the true VCD (Boersma et al., 2009b; Hains et al., 2009; Huijnen et al., personal communication, 2009; Lamsal et al., 2009; Zhou et al., 2009). The resulting top-down emission budget for East China is 17% higher than the best estimate and 13% higher than the a priori. The second test (case 7) was to adjust GOME-2 and OMI retrievals independently before the top-down derivation. van Noije et al. (2006) compared the KNMI retrieval method for GOME with the other two independent methods at Bremen University (Richter and Burrows, 2002; Richter et al., 2005) and Dalhousie University/SAO (Martin et al., 2003). They found that the VCD in July 2000 retrieved by the three methods ranges from $\sim 2.5 \times 10^{15}$ molec/cm^2 (By Bremen University) to $\sim 5.1 \times 10^{15}$ molec/cm^2 (by KNMI) over northern East China (110°–123° E, 30°–40° N). Assuming the mean of VCD retrievals from the three methods as the true VCD, the KNMI retrieval for GOME would be overestimated by ~32% for July 2000. Assuming the GOME-2 retrieval here had the same level of error as GOME, it was reduced by 32% over China. A number of recent studies (Boersma

ACPD
9, 19205–19241, 2009

et al., 2009b; Hains et al., 2009; Huijnen et al., personal communication, 2009; Lamsal et al., 2009; Zhou et al., 2009) have suggested that the KNMI OMI retrieval is biased positively, most likely with a magnitude of 0–30% irrespective of season. Thus the OMI retrieval was reduced by 15% as a medium modification. The top-down results using the adjusted GOME-2 and OMI retrievals showed a budget ~7% (~3%) larger than our best estimate (a priori) for East China. In the third test (case 8), NO_2 retrievals from SCIAMACHY by KNMI were used in place of GOME-2. The SCIAMACHY retrieval has been compared with OMI by Boersma et al. (2008b) for evaluating emission and chemical variations of tropospheric NO_2 for East China and other world regions. Combining SCIAMACHY and OMI using our approach lead to a top-down emission budget for East China that is ~9% (~5%) higher than our best estimate (a priori). In conclusion, we find our best estimate provides relatively robust information on Chinese anthropogenic emissions. Systematic errors in both retrievals may lead to underestimation in our best estimate by at most 17% (mostly likely ≤10%).

Second, GEOS-Chem simulations may be subject to systematic errors. The non-local PBL mixing scheme is expected to improve the simulated vertical profiles of NO_2. A sensitivity simulation assuming full PBL mixing leads to ~4% increase in the top-down emission budget (case 9). However, the non-local scheme may still fail to simulate the PBL mixing accurately due to the relatively coarse spatial resolution of the model. Also, the monthly climatology assumed for lightning may not be able to represent the real world due to its large interannual variability, introducing thus potential biases in the top-down constraint since lightning is an important source of NO_x. A sensitivity simulation doubling lightning emissions results in ~15% reduction in the anthropogenic emission budget (case 10). Additionally, this study also uses the INTEX-B emissions for carbon monoxide (CO) and volatile organic compounds (VOCs), which could differ from the actual emissions in 2008 resulting in errors in the simulated OH and thus the NO_x lifetime. Another sensitivity simulation (case 11), with anthropogenic CO and VOC emissions increased by 50%, indicates that the modeled OH column and NO_x lifetime are affected by less than 4%, and that the top-down emission budget for

East China is reduced by ~3%. Furthermore, the a priori emissions do not have diurnal variation when used in the GEOS-Chem simulation for calculating τ and $\Omega_{NO_x,r}$, with the assumption that these two quantities are independent of NO_x emissions. In another sensitivity test (case 12), our best estimate of emission diurnal profiles (Fig. 4) was applied to the a priori and the GEOS-Chem simulation was re-run. As a result, τ and $\Omega_{NO_x,r}$ are affected by less than 3%, while the top-down emission budget is increased by ~9%.

The third factor relates to the assumptions on the diurnal profiles of emissions and the uncertainties in overall budgets across the four sectors. The single diurnal variation curve for each sector cannot distinguish individual sub-sectors (vehicle types, factory sizes, etc.), locations, or day-to-day variability. Two additional scenarios were designed to test the impacts of emission diurnal variation assumptions. In one scenario (case 4), we assumed that emissions were constant with time for all sectors and obtained an "upper limit" to the top-down emissions. In another (case 5), we assumed that the diurnal variations for all sectors followed the US EPA 1989 estimation (Fig. 4), with emissions from 6:00 a.m. to 2:00 p.m. 35% higher than the daily mean. This results in a "lower limit" for top-down emissions, since total Chinese anthropogenic emissions are not expected to exhibit such a large diurnal variation. Anthropogenic emission budgets for the two scenarios are 6.6 and 4.9 Tg N/yr, respectively, for East China (Table 2). Additionally, the budget uncertainty estimate for the four sectors is preliminary, particularly since it was derived for national budgets but is applied here to all locations. A sensitivity test (case 13), with uncertainty of power plant emissions increased by 50%, showed impacts on the contributions of each sector to individual locations, but not on their national budgets (Table 2).

Fourth, the top-down constraint is affected by the assumptions on soil emissions. To evaluate this, two additional cases were implemented to test each of the "best estimate", "upper limit" and "lower limit" scenarios, where soil emissions are assumed to be either (1) the same as or (2) tripling the a priori (case 14–19). The resulting top-down anthropogenic emission budgets are within 10% of the corresponding scenarios

ACPD
9, 19205–19241, 2009

(Table 2).

Figure 8 summarizes the aforementioned uncertainties in our top-down estimate as a histogram plot. It is shown that the top-down emission budget is within 15% of our best estimate in 13 (12) out of the total 17 sensitivity cases for the whole country (East China). The standard deviation over all cases is ~13% of the best estimate emission budget. The total uncertainty in our best top-down estimate may be larger than 13%, since the sensitivity cases analyzed here are not completely independent. Therefore the uncertainty is estimated here with an alternate approach. It is approximated as the standard deviation of the top-down estimations derived for individual days of the month divided by the top-down estimation using the monthly-mean columns. Similar approximations have been used in previous studies (e.g., Wang et al., 2004). An additional 30% error is added tentatively to account further for impacts of systematic errors in retrievals and model results persistent in July 2008. Figure 6b shows that uncertainties in the top-down total anthropogenic emissions are less than 60% in most regions. The large uncertainties in several sparse locations correspond often to low emissions in both top-down and a priori datasets.

The a posteriori emissions relative to the best top-down estimate are derived for each sector together with the total (Fig. 5), using uncertainties in the top-down and a priori emissions to determine their relative contributions (Martin et al., 2003). The resulting emission budget is 5.7 Tg N/yr over East China and 6.8 Tg N/yr for the whole country (Table 2). The uncertainties for total anthropogenic emissions are 45% or less over most regions (Fig. 6d). The national budget here is ~10% less than the a posteriori estimate of 7.5 Tg N/yr for July 2007 by Zhao and Wang (2009). This may be a result of different time of interest (July 2008, with more emission restriction due to the Olympics, versus July 2007), different estimate methods (the newly proposed approach applied to monthly means versus the Martin et al. approach applied to daily assimilation), different retrievals (the KNMI retrieval versus the mean of KNMI and NASA retrievals) and/or different resolutions.

ACPD

9, 19205–19241, 2009

6 Conclusions and discussions

The methodology introduced here offers an improvement on the Martin et al. method (Martin et al., 2003) for constraining anthropogenic emissions. By incorporating GEOS-Chem with multiple satellite retrievals and accounting for diurnal variations of different anthropogenic sectors, it not only improves the constraint of daily mean total anthropogenic emissions, but is able also to simultaneously constrain individual sectors, which as a result improves the quantification of the diurnal variation of total anthropogenic emissions.

The best top-down estimate leads to an anthropogenic emission budget of about 5.5 Tg N/yr over East China for July 2008, comparable to 5.7 Tg N/yr in the a priori. The national budgets are 6.8 Tg N/yr and 6.6 Tg N/yr in the top-down and a priori datasets, respectively. These small differences are possibly as a result of the rapid pace of industrialization and urbanization balanced to a large extent by the emission control efforts in recent years. The top-down emissions are smaller than the a priori near Beijing, in the northeastern provinces and along the east coast. They, however, exceed the a priori over many inland regions. Differences in systematic errors between individual retrievals may lead to underestimation of top-down emissions by at most 17% (most likely $\leq$10%). Impacts of errors and uncertainties in GEOS-Chem and methodology are analyzed by a suite of sensitivity tests. The standard deviation of all sensitivity cases is only $\sim$13% of the top-down emission budget derived from our best estimate. The a posteriori emissions corresponding to the best top-down estimate suggest a national budget of 6.8 Tg N/yr (5.7 Tg N/yr in East China).

A key assumption in both methods is the neglect of horizontal transport. Thus, even in summer, it is important to avoid incorporating the nighttime evolution of NO_x, since its lifetime is relatively longer allowing for more effective transport. Since the Martin et al. method is restricted to analysis of a single satellite retrieval, their results depend implicitly on the treatment of the nighttime evolution of NO_x (see Sect. 2). By comparison, using multiple retrievals, the present approach accounts for the evolution of

ACPD
9, 19205–19241, 2009

NO_x in the daytime (10:00 a.m.-2:00 p.m.), when its lifetime is relatively short and when the neglect of horizontal transport is likely to be less problematic. Also, the quantities required from the model in the present study, including the ratio between NO_x and NO_2 columns and the lifetime of NO_x in the daytime, are insensitive to the treatment of NO_x during nighttime. If the methodology were to be applied to wintertime when photochemistry is less efficient and the lifetime of NO_x is longer, additional measures may be needed to account appropriately for the effects of horizontal transport.

Acknowledgement. This research is supported by the National Science Foundation, grant ATM-0635548. We thank Xueyuan Wang, Lee Murray, Yu Zhao and Yu Lei for their help and for informative discussions. We acknowledge the free use of tropospheric NO_2 column data from GOME-2 and OMI from http://www.temis.nl.

References

Acarreta, J. R., De Haan, J. F., and Stammes, P.: Cloud pressure retrieval using the O_2–O_2 absorption band at 477 nm, J. Geophys. Res., 109, D05204, doi:10.1029/2003jd003915, 2004.

Boersma, K. F., Eskes, H. J., and Brinksma, E. J.: Error analysis for tropospheric NO_2 retrieval from space, J. Geophys. Res., 109, D04311, doi:10.1029/2003jd003962, 2004.

Boersma, K. F., Eskes, H. J., Veefkind, J. P., Brinksma, E. J., van der A, R. J., Sneep, M., van den Oord, G. H. J., Levelt, P. F., Stammes, P., Gleason, J. F., and Bucsela, E. J.: Near-real time retrieval of tropospheric NO_2 from OMI, Atmos. Chem. Phys., 7, 2103–2118, 2007, http://www.atmos-chem-phys.net/7/2103/2007/.

Boersma, K. F., Jacob, D. J., Bucsela, E. J., Perring, A. E., Dirksen, R., van der A, R. J., Yantosca, R. M., Park, R. J., Wenig, M. O., Bertram, T. H., and Cohen, R. C.: Validation of OMI tropospheric NO_2 observations during INTEX-B and application to constrain NO_x emissions over the eastern United States and Mexico, Atmos. Environ., 42, 4480–4497, doi:10.1016/j.atmosenv.2008.02.004, 2008a.

Boersma, K. F., Jacob, D. J., Eskes, H. J., Pinder, R. W., Wang, J., and van der A, R. J.: Intercomparison of SCIAMACHY and OMI tropospheric NO_2 columns: Observing the di-

urnal evolution of chemistry and emissions from space, J. Geophys. Res., 113, D16S26, doi:10.1029/2007jd008816, 2008b.
Boersma, K. F., Dirksen, R., Veefkind, J. P., Eskes, H. J., and van der A, R. J.: Dutch OMI NO2 (DOMINO) data product HE5 data file user manual, 17 p., available at http://www.temis.nl/docs/OMI_NO2_HE5_1.0.2.pdf, 2009a.
Boersma, K. F., Jacob, D. J., Trainic, M., Rudich, Y., DeSmedt, I., Dirksen, R., and Eskes, H. J.: Validation of urban NO_2 concentrations and their diurnal and seasonal variations observed from space sensors using in situ measurements in Israeli cities, Atmos. Chem. Phys., 9, 3867–3879, 2009b, http://www.atmos-chem-phys.net/9/3867/2009/.
Chen, D., Wang, Y., McElroy, M. B., He, K., Yantosca, R. M., and Sager, P. L.: Regional CO pollution in China simulated by the high-resolution nested-grid GEOS-Chem model, Atmos. Chem. Phys. Discuss., 9, 5853–5887, 2009, http://www.atmos-chem-phys-discuss.net/9/5853/2009/.
Hains, J., Boersma, F., Kroon, M., Dirksen, R., Volten, H., Swart, D., Richter, A., Wittrock, F., Schoenhardt, A., Wagner, T., Ibrahim, O., Roozendael, M. v., Pinardi, G., Gleason, J., Veefkind, P., and Levelt, P.: Testing and improving OMI DOMINO tropospheric NO_2 using observations from the DANDELIONS and INTEX-B validation campaigns, J. Geophys. Res., submitted, doi:10.1029/2009JD012399, 2009.
Holtslag, A. A. M. and Boville, B. A.: Local versus nonlocal boundary-layer diffusion in a global climate model, J. Climate, 6, 1825–1842, 1993.
Jaeglé, L., Steinberger, L., Martin, R. V., and Chance, K.: Global partitioning of NO_x sources using satellite observations: Relative roles of fossil fuel combustion, biomass burning and soil emissions, Faraday Discuss., 130, 407–423, doi:10.1039/b502128f, 2005.
Lamsal, L., Martin, R., and v. Donkelaar, A.: Seasonal variation in nitrogen oxides at northern midlatitudes as inferred from ground-based and satellite-based observations, GEOS-Chem Meeting, April 2008, 2009.
Lin, J. T., Wuebbles, D. J., and Liang, X. Z.: Effects of intercontinental transport on surface ozone over the United States: Present and future assessment with a global model, Geophys. Res. Lett., 35, L02805, doi:10.1029/2007gl031415, 2008a.
Lin, J. T., Youn, D., Liang, X. Z., and Wuebbles, D. J.: Global model simulation of summertime US ozone diurnal cycle and its sensitivity to PBL mixing, spatial resolution, and emissions, Atmos. Environ., 42, 8470–8483, doi:10.1016/j.atmosenv.2008.08.012, 2008b.

ACPD
9, 19205–19241, 2009

Martin, R. V., Jacob, D. J., Chance, K., Kurosu, T. P., Palmer, P. I., and Evans, M. J.: Global inventory of nitrogen oxide emissions constrained by space-based observations of NO_2 columns, J. Geophys. Res., 108, 4537, doi:10.1029/2003jd003453, 2003.

Martin, R. V., Sioris, C. E., Chance, K., Ryerson, T. B., Bertram, T. H., Wooldridge, P. J., Cohen, R. C., Neuman, J. A., Swanson, A., and Flocke, F. M.: Evaluation of space-based constraints on global nitrogen oxide emissions with regional aircraft measurements over and downwind of eastern North America, J. Geophys. Res., 111, D15308, doi:10.1029/2005jd006680, 2006.

McElroy, M. B. and Wang, Y. X. X.: Human and animal wastes: Implications for atmospheric N_2O and NO_x, Global Biogeochem. Cy., 19, GB2008, doi:10.1029/2004gb002429, 2005.

Mijling, B., van der A, R. J., Boersma, K. F., Roozendael, M. V., DeSmedt, I., and Kelder, H. M.: Reductions of NO2 detected from space during the 2008 Beijing Olympic Games, Geophys. Res. Lett., 36, L13801, doi:10.1029/2009GL038943, 2009.

Pickering, K. E., Wang, Y. S., Tao, W. K., Price, C., and Muller, J. F.: Vertical distributions of lightning NOx for use in regional and global chemical transport models, J. Geophys. Res., 103, 31203–31216, 1998.

Price, C., Penner, J., and Prather, M.: NO_x from lightning. 1. Global distribution based on lightning physics, J. Geophys. Res., 102, 5929–5941, 1997.

Richter, A., and Burrows, J. P.: Tropospheric NO2 from GOME measurements, Adv. Space Res., 29, 1673–1683, 2002.

Richter, A., Burrows, J. P., Nuss, H., Granier, C., and Niemeier, U.: Increase in tropospheric nitrogen dioxide over China observed from space, Nature, 437, 129–132, doi:10.1038/nature04092, 2005.

Sauvage, B., Martin, R. V., van Donkelaar, A., Liu, X., Chance, K., Jaeglé, L., Palmer, P. I., Wu, S., and Fu, T. M.: Remote sensed and in situ constraints on processes affecting tropical tropospheric ozone, Atmos. Chem. Phys., 7, 815–838, 2007, http://www.atmos-chem-phys.net/7/815/2007/.

Streets, D. G., Bond, T. C., Carmichael, G. R., Fernandes, S. D., Fu, Q., He, D., Klimont, Z., Nelson, S. M., Tsai, N. Y., Wang, M. Q., Woo, J. H., and Yarber, K. F.: An inventory of gaseous and primary aerosol emissions in Asia in the year 2000, J. Geophys. Res., 108, 8809, doi:10.1029/2002jd003093, 2003.

van der A, R. J., Eskes, H. J., Boersma, K. F., van Noije, T. P. C., Van Roozendael, M., De Smedt, I., Peters, D., and Meijer, E. W.: Trends, seasonal variability and dominant NOx

source derived from a ten year record of NO_2 measured from space, J. Geophys. Res., 113, D04302, doi:10.1029/2007jd009021, 2008.

Wang, P., Stammes, P., van der A, R. J., Pinardi, G., and Roozendael, M. v.: FRESCO+: an improved O_2 A-band cloud retrieval algorithm for tropospheric trace gas retrievals, Atmos. Chem. Phys., 8, 9697–9729, 2008, http://www.atmos-chem-phys.net/8/9697/2008/.

Wang, X. P., Mauzerall, D. L., Hu, Y. T., Russell, A. G., Larson, E. D., Woo, J. H., Streets, D. G., and Guenther, A.: A high-resolution emission inventory for eastern China in 2000 and three scenarios for 2020, Atmos. Environ., 39, 5917–5933, doi:10.1016/j.atmonsenv.2005.06.051, 2005.

Wang, Y. X., McElroy, M. B., Martin, R. V., Streets, D. G., Zhang, Q., and Fu, T. M.: Seasonal variability of NO_x emissions over east China constrained by satellite observations: Implications for combustion and microbial sources, J. Geophys. Res., 112, D06301, doi:10.1029/2006jd007538, 2007.

Wang, Y. X. X., McElroy, M. B., Wang, T., and Palmer, P. I.: Asian emissions of CO and NOx: Constraints from aircraft and Chinese station data, J. Geophys. Res., 109, D24304, doi:10.1029/2004jd005250, 2004.

Wuebbles, D. J., Lei, H., and Lin, J. T.: Intercontinental transport of aerosols and photochemical oxidants from Asia and its consequences, Environ. Pollut., 150, 65–84, doi:10.1016/j.envpol.2007.06.066, 2007.

Yienger, J. J., and Levy, H.: Empirical-model of global soil-biogenic NO_x emissions, J. Geophys. Res., 100, 11447–11464, 1995.

Zhang, L., Jacob, D. J., Boersma, K. F., Jaffe, D. A., Olson, J. R., Bowman, K. W., Worden, J. R., Thompson, A. M., Avery, M. A., Cohen, R. C., Dibb, J. E., Flock, F. M., Fuelberg, H. E., Huey, L. G., McMillan, W. W., Singh, H. B., and Weinheimer, A. J.: Transpacific transport of ozone pollution and the effect of recent Asian emission increases on air quality in North America: an integrated analysis using satellite, aircraft, ozonesonde, and surface observations, Atmos. Chem. Phys., 8, 6117–6136, 2008, http://www.atmos-chem-phys.net/8/6117/2008/.

Zhang, Q., Streets, D. G., He, K., Wang, Y., Richter, A., Burrows, J. P., Uno, I., Jang, C. J., Chen, D., Yao, Z., and Lei, Y.: NO_x emission trends for China, 1995–2004: The view from the ground and the view from space, J. Geophys. Res., 112, D22306, doi:10.1029/2007jd008684, 2007.

Zhang, Q., Streets, D. G., and He, K.: Satellite observations of recent power plant construction

ACPD

9, 19205–19241, 2009

in Inner Mongolia, China, Geophys. Res. Lett., 36, L15809, doi:10.1029/2009GL038984, 2009.

Zhang, Q., Streets, D. G., Carmichael, G. R., He, K., Huo, H., Kannari, A., Klimont, Z., Park, I., Reddy, S., Fu, J. S., Chen, D., Duan, L., Lei, Y., Wang, L., and Yao, Z.: Asian emissions in 2006 for the NASA INTEX-B mission, Atmos. Chem. Phys., 9, 5131–5153, 2009, http://www.atmos-chem-phys.net/9/5131/2009/.

Zhao, C., and Wang, Y. H.: Assimilated inversion of NOx emissions over east Asia using OMI NO_2 column measurements, Geophys. Res. Lett., 36, L06805, doi:10.1029/2008gl037123, 2009.

Zhou, Y., Brunner, D., Boersma, K. F., Dirksen, R., and Wang, P.: An improved tropospheric NO_2 retrieval for satellite observations in the vicinity of mountainous terrain, Atmos. Meas. Tech. Discuss., 2, 401–416, 2009, http://www.atmos-meas-tech-discuss.net/2/401/2009/.

Table 1. Properties of Level-2 NO_2 retrievals from GOME-2 and OMI[a]

.

Instrument	Onboard satellite	Local equator crossing time	Nadir view resolution	Viewing swath	Global coverage	Retrieval version
GOME-2	MetOp-A	9:30 a.m.	40×80 km^2	1500 km	~1 d	TM4NO2A v1.10
OMI	EOS-Aura	1:30 p.m.	13×24 km^2	2600 km	1 d	DOMINO v1.0.2

[a] See more information at http://www.temis.nl/airpollution/no2.html.

ACPD

9, 19205–19241, 2009

Table 2. Annual anthropogenic emission budgets (Tg N/yr) of NO_x in China[a]

.

Case	Description[b]	China					East China (103.75°–123.75° E, 19°–45° N)[c]				
		total	ind	pow	mob	res	total	ind	pow	mob	res
(1) a priori	a priori	6.6	1.7	2.9	1.7	0.4	5.7	1.5	2.5	1.4	0.3
(2) TD:[d] best estimate	best estimate	6.8	1.7	2.9	1.8	0.5	5.5	1.4	2.4	1.3	0.3
(3) a posteriori	relative to (2)	6.8	1.7	2.9	1.7	0.5	5.7	1.5	2.5	1.4	0.3
(4) TD: upper limit	no emission diurnal variations	8.2	2.0	3.3	2.1	0.8	6.6	1.7	2.8	1.6	0.5
(5) TD: lower limit	emission variations use the US EPA 1989 estimation	6.1	1.5	2.6	1.6	0.4	4.9	1.2	2.2	1.2	0.2
(6) TD: adj_GOME-2	GOME-2 scaled down by 113%	8.0	2.0	3.2	2.1	0.7	6.4	1.6	2.7	1.6	0.5
(7) TD: adj_GOME-2 & OMI	GOME-2 reduced by 32% and OMI reduced by 15%	7.3	1.8	3.0	1.9	0.6	5.8	1.5	2.5	1.4	0.4
(8) TD: SCIA+OMI	SCIAMACHY in place of GOME-2	7.3	1.8	3.0	1.9	0.6	6.0	1.5	2.6	1.5	0.4
(9) TD: fullmix	assume full mixing PBL	7.1	1.8	3.0	1.8	0.6	5.7	1.5	2.5	1.4	0.4
(10) TD: 2×lgt	lightning NO_x emissions doubled	5.8	1.4	2.5	1.5	0.4	4.6	1.2	2.1	1.1	0.2
(11) TD: 1.5×HC	anthropogenic emissions of CO and VOCs increased by 50%	6.7	1.6	2.8	1.7	0.5	5.3	1.3	2.3	1.3	0.3
(12) TD: dv_emis	best estimate emission diurnal variations applied to the a priori	7.4	1.8	3.0	1.9	0.6	6.0	1.5	2.6	1.5	0.4
(13) TD: 1.5×pow	budget uncertainty for power plants increased by 50%	6.8	1.7	2.9	1.8	0.5	5.5	1.4	2.4	1.3	0.3
Sensitivity to assumed soil emissions											
(14) TD: 1×soil	similar to (2), but with soil emissions unchanged	7.5	1.8	3.1	1.9	0.6	6.0	1.5	2.6	1.5	0.4
(15) TD: 3×soil	similar to (2), but with soil emissions tripled	6.2	1.5	2.6	1.6	0.5	5.0	1.3	2.2	1.2	0.3
(16) TD: UL+1×soil	similar to (4), but with soil emissions unchanged	9.0	2.2	3.6	2.3	0.9	7.2	1.8	3.0	1.8	0.6
(17) TD: UL+3×soil	similar to (4), but with soil emissions tripled	7.4	1.8	3.0	1.9	0.6	6.0	1.5	2.5	1.5	0.4
(18) TD: LL+1×soil	similar to (5), but with soil emissions unchanged	6.7	1.6	2.8	1.7	0.5	5.3	1.3	2.4	1.3	0.3
(19) TD: LL+3×soil	similar to (5), but with soil emissions tripled	5.5	1.4	2.4	1.5	0.3	4.4	1.1	2.0	1.1	0.2

[a] Assuming no seasonal variations. Emissions include total anthropogenic sources ("total") and all four sectors: industry ("ind"), power plants ("pow"), mobile ("mob") and residential ("res").
[b] Descriptions for Case (4–15) only show differences from the best estimate (Case (2)).
[c] Gridcells not occupied by Chinese lands are not included for calculating the total.
[d] Top-down.

ACPD
9, 19205–19241, 2009

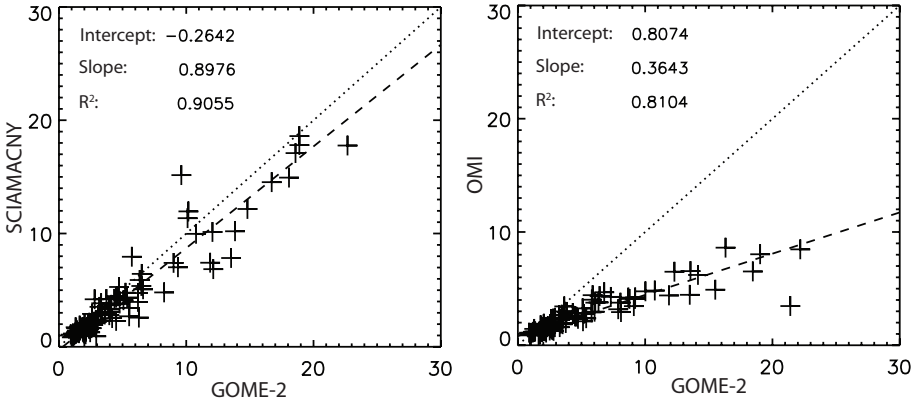

Fig. 1. Scatter plot ("pluses") for the spatial distributions of monthly mean tropospheric NO_2 columns (10^{15} molec/cm^2) from different retrievals over East China in July 2008. Results from the RMA regression are provided as well. The dashed line is the fit to the data, and the dotted line denotes the 1:1 ratio.

ACPD
9, 19205–19241, 2009

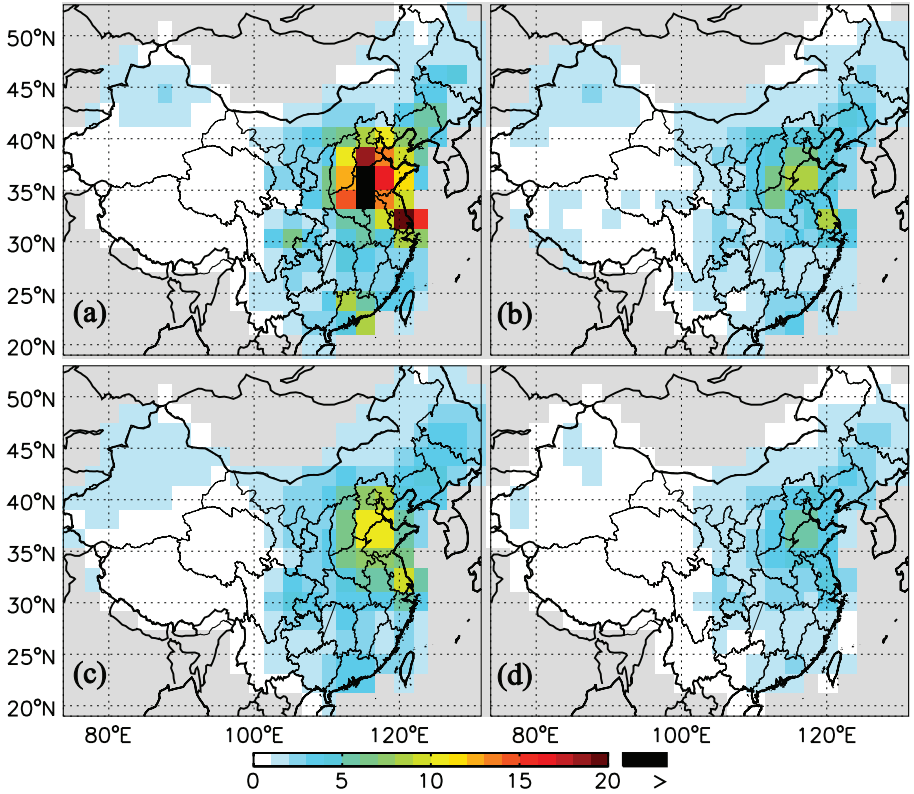

Fig. 2. Tropospheric NO_2 column concentrations (10^{15} molec/cm^2) for July 2008 retrieved by **(a)** GOME-2 and **(b)** OMI, and corresponding GEOS-Chem simulations in **(c)** for 10:00 a.m. and **(d)** 2:00 p.m., respectively.

ACPD
9, 19205–19241, 2009

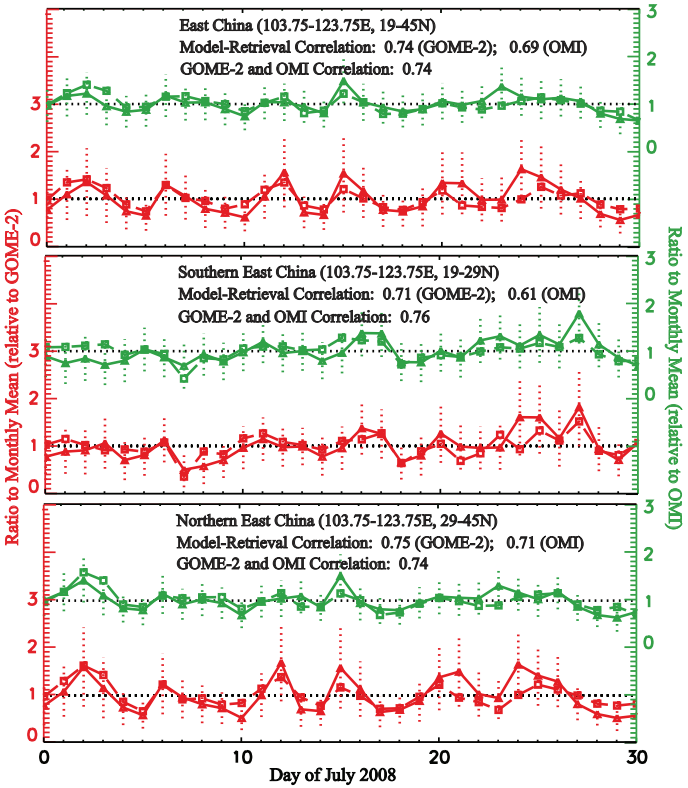

Fig. 3. Normalized (i.e., divided by monthly mean) daily variations of retrieved (solid lines with "triangle" symbols) and simulated (dashed lines with "square" symbols) tropospheric NO_2 column concentrations in July 2008 for East China and its southern and northern portions. Red lines correspond to GOME-2 and green lines OMI. Dotted vertical lines indicate the standard deviations of retrievals. Daily retrieval-simulation correlations are also shown.

ACPD
9, 19205–19241, 2009

Satellite constraint of anthropogenic NO_x emissions in China from different sectors

J.-T. Lin et al.

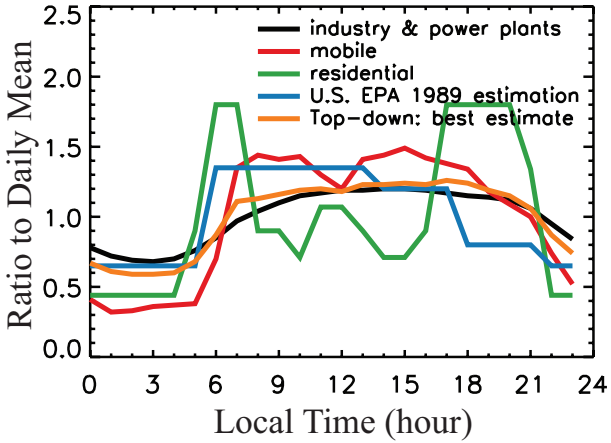

Fig. 4. Estimated diurnal profiles of Chinese anthropogenic emissions from individual sectors (black, red and green lines), the US EPA 1989 estimate (blue line), and the profile corresponding to our best top-down estimate of total anthropogenic emissions in East China (orange line).

ACPD
9, 19205–19241, 2009

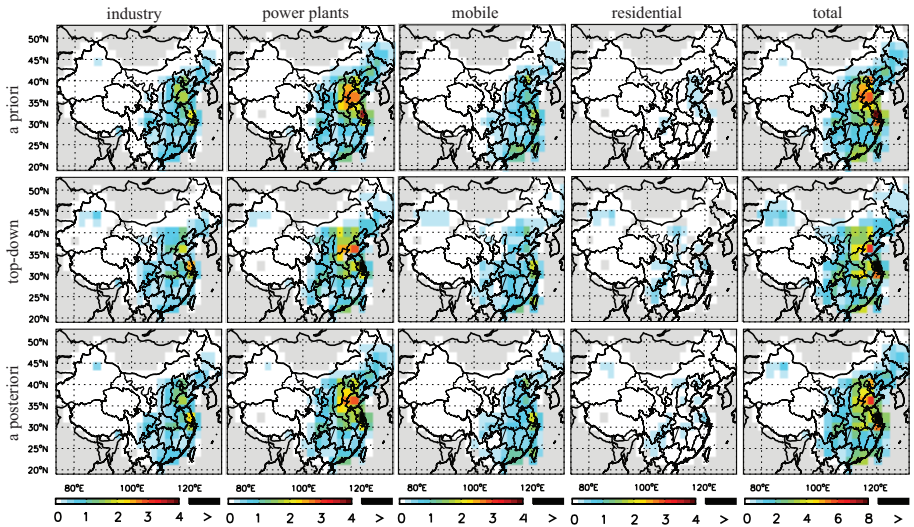

Fig. 5. Chinese anthropogenic emissions of NO_x (kg N/s) from four major sectors and their total in the a priori, top-down and a posteriori datasets. Top-down and a posteriori emissions are kept the same as the a priori for gridcells with either GOME-2 or OMI retrievals less than 1×10^{15} molec/cm^2 (mostly in the western provinces). Gridcells not occupied by Chinese lands or with zero emissions are masked out as gray.

ACPD

9, 19205–19241, 2009

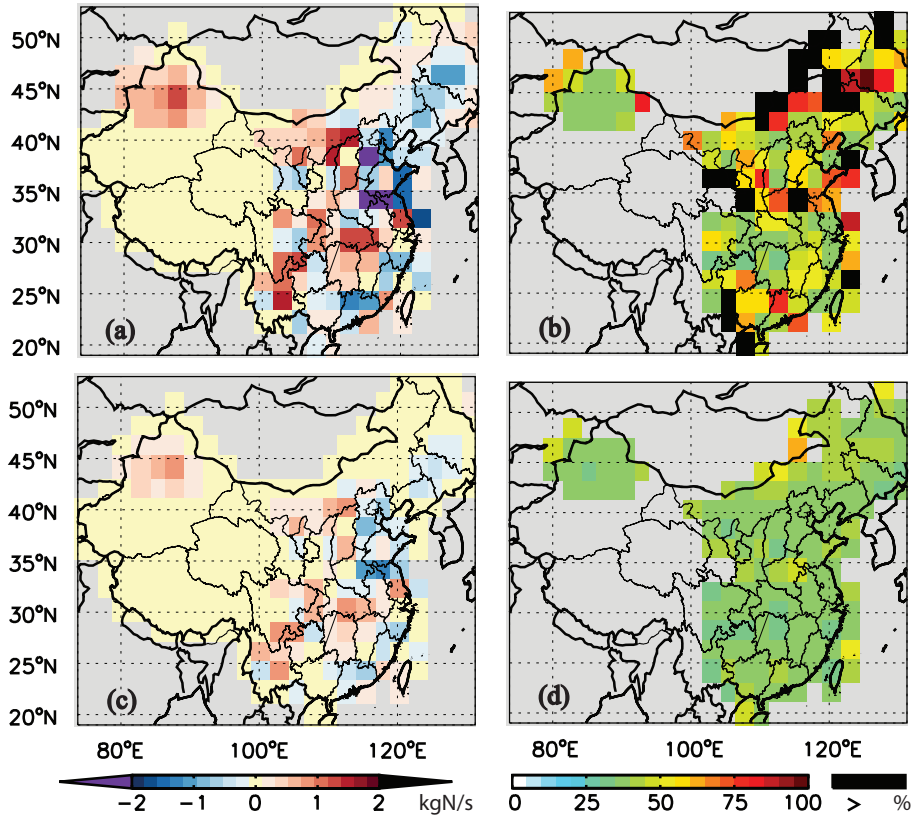

Fig. 6. Differences in total anthropogenic emissions between our best top-down estimate and the a priori datasets (i.e., top-down minus a priori) **(a)** and relative uncertainties in the top-down emissions **(b)** over China in July 2008; and the corresponding differences between the a posteriori and the a priori datasets (i.e., a posteriori minus a priori) **(c)** and relative uncertainties in the a posteriori emissions **(d)**.

ACPD
9, 19205–19241, 2009

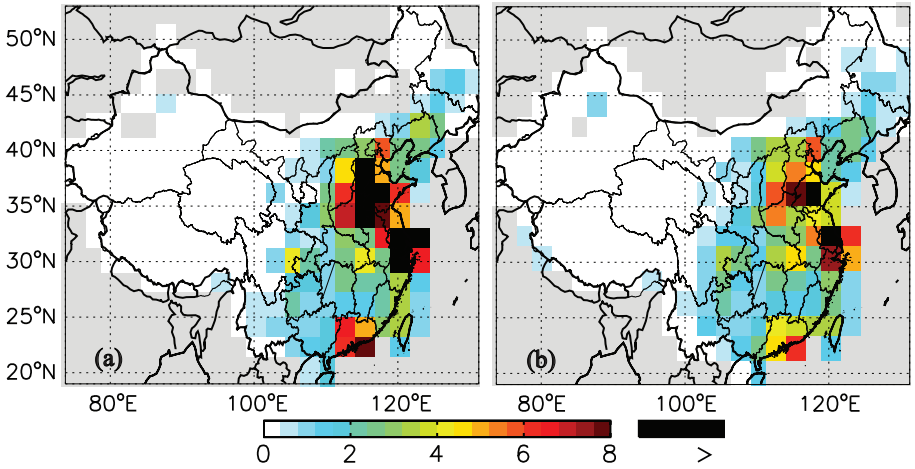

Fig. 7. Top-down total anthropogenic emissions of NO_x (kg N/s) for July 2008 derived with the Martin et al. method, using the **(a)** GOME-2 and **(b)** OMI retrievals. Soil emissions are doubled for deriving these anthropogenic emissions. Emissions are kept the same as the a priori for gridcells with retrievals less than 10^{15} molec/cm^2 (mostly in the western provinces). Gridcells not occupied by Chinese lands or with zero emissions are masked out as gray.

ACPD
9, 19205–19241, 2009

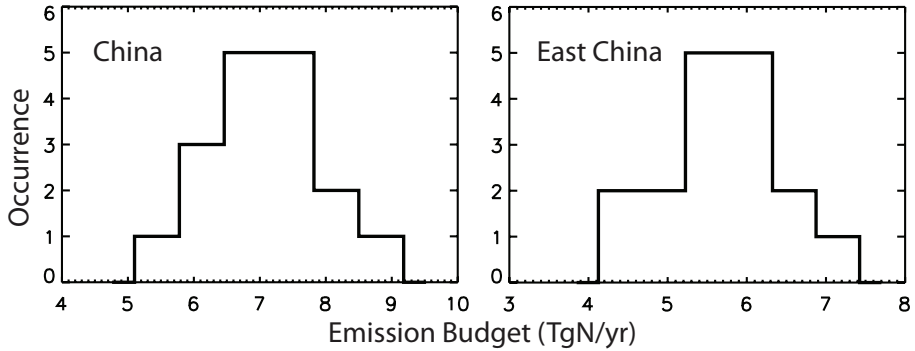

Fig. 8. Histogram plot of top-down emission budgets in the 17 different cases described in Table 2. Cases (1) and (3) represent the a priori and a posteriori, respectively, and are not included here.

ACPD

9, 19205–19241, 2009